NOVEMBER 08 2021

On sound propagation along an infinite rectangular duct-like structure with a finite slot opening and its modelling

S. H. K. Chu; S. K. Tang

J. Acoust. Soc. Am. 150, 3445–3460 (2021)
https://doi.org/10.1121/10.0007061

JASA ARTICLE

On sound propagation along an infinite rectangular duct-like structure with a finite slot opening and its modelling

S. H. K. Chu[a] and S. K. Tang[b]
Department of Building Environment and Energy Engineering, The Hong Kong Polytechnic University, Hong Kong, China

ABSTRACT:
The sound propagation across a sound leaking section along an infinite rectangular duct-like structure near to the lower order duct eigenfrequencies is investigated numerically in the present study. The sound leakage is achieved by finite length rectangular slots located at a corner of the duct-like structure cross section. The finite-element simulations are performed, in the first place, to gain insights into the modal development inside the structure. A semi-analytical model, which considers the wavy air motions along the slots with oblique sound radiation patterns, is developed. An empirical framework is also proposed to estimate the complex longitudinal wavenumber along the slot using the numerical results and dimensional analysis. The performance of the proposed semi-analytical model, together with the complex wavenumber prediction framework, is tested using two duct-like structures with different cross section aspect ratios. The results show that the present proposed approach gives predictions close to the finite-element simulations. The deviations are well within engineering tolerance. © *2021 Acoustical Society of America*.
https://doi.org/10.1121/10.0007061
(Received 22 August 2021; revised 9 October 2021; accepted 12 October 2021; published online 8 November 2021)
[Editor: Lixi Huang] Pages: 3445–3460

I. INTRODUCTION

Duct-like structures are important elements in many branches of engineering and, thus, have been studied extensively in the past few decades (for instance, the air conditioning and ventilation system ductwork[1] and corridors inside a building complex[2]). However, work related to a sound-leak duct-like structure is rarely found in the existing literature. In fact, these structures are not uncommon in practice. There are corridors/hallways in the perimeter zones of buildings where top-hung windows/louvres are installed above fixed windows on the building façade.[3] The tube-like cavity underneath the working platform in a train viaduct is another example.[4] There are studies related to the detection of leakage in a flow duct, for instance, Xu *et al.*[5] and Xiao *et al.*[6] However, the size of the sound leaking opening considered in these two studies is very small. There are also investigations which look into the change in the duct frequency responses caused by duct leakages of different sizes[7] and the mechanisms behind the change.[8,9] However, only normal duct modes are considered.

Although the energy of a sound wave will decrease with increasing downstream distance as it propagates along a sound-leak duct, in general, the sounds at frequencies near to the eigenfrequencies of the duct, especially those of lower orders, could travel over long distances before they become insignificant. However, for a sound leaking section with a finite length, these sounds will dominate the sound field in the duct section downstream of the sound-leak section. The strengths of these acoustic modes and their relationships with the dimensions of the duct and sound leaking slot are not well investigated. This forms one of the major objectives of this study.

Apart from gaining understanding of the sound field development, this study is also focussed on the development of a simplified prediction model for the sound propagation along an infinite duct with a finite length sound-leak section. For simplicity, a rectangular slot of finite length is opened near to a corner of the duct-like structure cross section for the leakage of sound. The widths of the slots tested are not large compared to the main duct width, therefore, the sound leakage is not too strong for the kind of modal analysis commonly adopted in a duct acoustics study (for instance, Cummings[10] and Tang and Tang[11]). The finite-element simulations are performed, in the first place, for understanding the sound propagation phenomenon as in many studies in the existing literature, such as in Hart and Lau[12] and Tang.[13] The corresponding results are also used to validate the newly developed sound propagation model. The present results not only reveal the acoustic mode development and sound power propagation along a sound-leak duct-like structure, which is a topic not fully explored in the existing literature, at least to the knowledge of the authors, but also enable quick and reasonably accurate prediction of the sound fields inside similar duct-like structures.

II. NUMERICAL SIMULATION SETUP

Figure 1 illustrates the schematics of the rectangular sound-leak duct and nomenclature adopted in the present

[a]Present address: Far East Consulting Engineers Limited, 12/F, Greenwich Centre, 260 King's Road, Hong Kong. Electronic mail: stevenhk.chu@connect.polyu.hk
[b]Electronic mail: shiu-keung.tang@polyu.edu.hk, ORCID: 0000-0002-0244-0224.

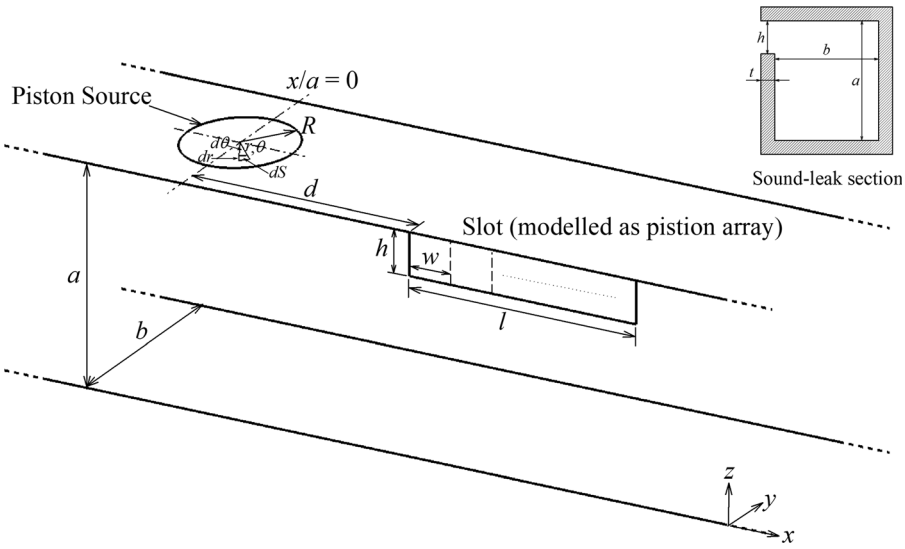

FIG. 1. The schematics of the sound-leak duct-like structure and nomenclature are shown.

study. The sound source takes the form of a circular piston of radius R mounted flush with the upper duct walls. The width and span of the duct cross section are represented by a and b, respectively. To avoid degenerate duct modes, b is set equal to ea/π, where e is the exponent number.[14] The height of the slot is h and its length is l. The thickness of the duct wall is t.

The finite-element method (FEM), implemented using COMSOL,[15] is used to solve the three-dimensional Helmholtz equation. The computational domains are presented in Fig. 2. A perfectly matched section is specified at each end of the duct section of interest to simulate the boundary condition of an infinitely long duct. A similar matched layer enclosing the sound-leak region is added to reduce the numerical reflection from the boundary of the main computational domain. The centre of this layer coincides with that of the slot opening. The lengths of all of these perfectly matched sections and the radius of the computational region for sound radiation out of the slot exceed one-half and a full wavelength of the lowest frequency of interest, respectively, where reference is made to the results of Liu.[16] In the simulations, the maximum mesh size is kept at least less than 1/8 of the smallest wavelength considered in this study based on the results of Marburg.[17] The sensitivity tests have been performed. It is found that a further increase in the perfectly matched section thicknesses or further refinement of mesh size do not give rise to noticeable changes in the simulated results (not shown here). The walls of the duct are set acoustically hard.

Table I illustrates a summary of the various mesh types and the corresponding element quality adopted in the present finite-element simulation. Two mesh systems are used and each of them looks after a particular frequency range of the simulation. In general, the qualities of the mesh elements are satisfactory.[15]

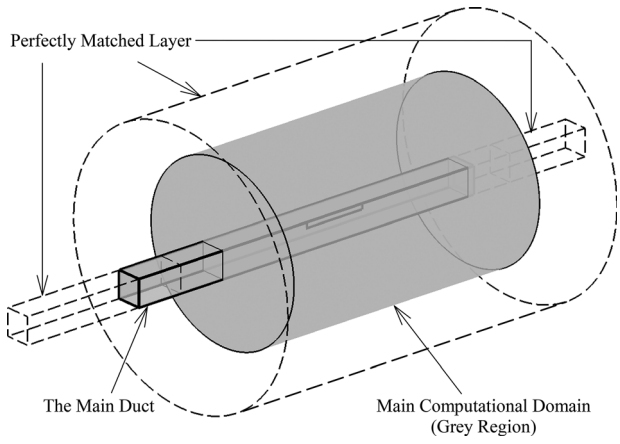

FIG. 2. The FEM computational domains (not drawn to scale) are shown.

III. THEORETICAL CONSIDERATION

Suppose that the piston source shown in Fig. 1 is centred at the point $(0,b/2,a)$ and vibrating with a velocity amplitude V and angular frequency ω, then the sound pressure p at any point (x,y,z) inside a straight rectangular duct without leakage so created is[18]

TABLE I. The summary of the mesh information and quality.

		Frequency range	
Mesh type	Mesh data	$0.1 < ka/\pi < 2.0$	$2.0 \le ka/\pi < 2.3$
Tetrahedral	Number of elements	417 555	915 469
	Minimum element quality	0.04634	0.02202
	Average element quality	0.7520	0.7569
	Maximum growth	3.630	3.934
	Average growth rate	1.632	1.613
	Element area ratio	2.62×10^{-6}	2.61×10^{-5}
Triangular	Number of elements	35 241	73 750
	Minimum element quality	0.2479	0.2444
	Average element quality	0.8594	0.8545
	Element area ratio	2.17×10^{-4}	9.93×10^{-4}
Edge	Number of elements	1649	2541
	Element length ratio	0.0207	0.0475
Vertex	Number of elements	72	74

https://doi.org/10.1121/10.0007061

$$p(x,y,z)=\frac{\rho V}{2ab}\sum_{m,n}c_{mn}\psi_{mn}(y,z)\times\oint\psi_{mn}(y',a)\left[H(x-x')e^{-i\omega(x-x')/c_{mn}}+H(x'-x)e^{i\omega(x-x')/c_{mn}}\right]dS, \quad (1)$$

with the normalized modal function for the (m,n) mode

$$\psi_{mn}(y,z)=\sqrt{(2-\delta_{0m})(2-\delta_{0n})}\cos\left(\frac{n\pi y}{b}\right)\cos\left(\frac{m\pi z}{a}\right), \quad (2)$$

and the modal wave speed

$$c_{mn}=\frac{\omega}{\sqrt{k^2-k_{mn}^2}}=\frac{\omega}{\sqrt{(\omega/c)^2-\pi^2\left[(m/a)^2+(n/b)^2\right]}}, \quad (3)$$

where k is the wavenumber ($=\omega/c$), k_{mn} is the modal wavenumber, m and n are non-negative integers, ρ is the ambient air density, H is the Heaviside step function, x' and y' are coordinates on the piston source surface S, $i=\sqrt{-1}$, δ is the delta function, and c is the ambient speed of sound. For $k<k_{mn}$, $\sqrt{k^2-k_{mn}^2}=-i\sqrt{|k^2-k_{mn}^2|}$ and, thus, $c_{mn}=i|c_{mn}|$. One can evaluate the integral in Eq. (1) analytically after expressing x' and y' in polar forms (see Appendix A). For $|x|>R$ and even n,

$$p(x,y,z)=\frac{\pi\rho\omega RV}{ab}\sum_{m,n}\sqrt{(2-\delta_{0m})(2-\delta_{0n})}\times\frac{(-1)^{m+n/2}J_1\left(R\sqrt{k^2-k_{m0}^2}\right)}{\sqrt{k^2-k_{mn}^2}\sqrt{k^2-k_{m0}^2}}\times\psi_{mn}(y,z)e^{-i\omega|x|/c_{mn}}, \quad (4)$$

where J_1 is the first-order Bessel function of the first kind. It should be noted that the integral in Eq. (1) vanishes for odd n. Only those acoustic modes which are symmetrical about the duct cross section central plane $y/b=0.5$ can exist inside the duct in the form of either a propagating wave or an evanescent wave.

The sound leaking slot in this study is approximated as a linear array of air pistons vibrating perpendicularly to the slot open surface with different vibration magnitudes, which are determined using the method adopted by Tang.[13] Suppose that the horizontal width of each piston is w (see Fig. 1), then the sound pressure p_j generated by the jth piston of the hypothetical piston array inside the duct can be estimated using Eq. (1) with S replaced by the air piston surface. Let x_j be the axial location of the centre of the jth piston, which is vibrating with a velocity amplitude V_j, one obtains for $|x-x_j|\geq w/2$

$$p_j=\frac{\rho\omega hV_j}{ab}\sum_{m,n}\sqrt{(2-\delta_{0m})(2-\delta_{0n})}(-1)^m\times\frac{\sin\left(\frac{m\pi}{a}h\right)}{\frac{m\pi}{a}h}\frac{\sin\left(\frac{\omega w}{2c_{mn}}\right)}{(k^2-k_{mn}^2)}\psi_{mn}(y,z)e^{-i\omega|x-x_j|/c_{mn}}. \quad (5)$$

For $|x-x_j|\leq w/2$,

$$p_j=\frac{\rho\omega hV_j}{ab}\sum_{m,n}\sqrt{(2-\delta_{0m})(2-\delta_{0n})}(-1)^m\times\frac{\sin\left(\frac{m\pi h}{a}\right)\left[1-e^{-i\omega w/2c_{mn}}\cos\left(\frac{\omega x}{c_{mn}}\right)\right]}{i\left(\frac{m\pi h}{a}\right)(k^2-k_{mn}^2)}\psi_{mn}(y,z). \quad (6)$$

There are three forces acting on the jth air piston. The first force results from the upstream sound from the piston source F_j, the second force is the fluid loading F_{sj}, and the third is the induced force F_{mj} caused by the vibrations of the other air pistons forming the slot,

$$F_j=\int_{x_j-w/2}^{x_j+w/2}\int_{a-h}^{a}p(x,0,z)\,dz\,dx, \quad (7a)$$

$$F_{sj}=V_j\int_{x_j-w/2}^{x_j+w/2}\int_{a-h}^{a}M(x,0,z|x_j)\,dz\,dx, \quad (7b)$$

$$F_{mj}=\sum_{i\neq j}V_i\int_{x_j-w/2}^{x_j+w/2}\int_{a-h}^{a}G(x,0,z|x_i)dzdx, \quad (7c)$$

where

$$G(x,y,z|x_j)=\frac{\rho\omega h}{ab}\sum_{m,n}\sqrt{(2-\delta_{0m})(2-\delta_{0n})}(-1)^m\times\frac{\sin\left(\frac{m\pi}{a}h\right)}{\frac{m\pi}{a}h}\frac{\sin\left(\frac{\omega w}{2c_{mn}}\right)}{(k^2-k_{mn}^2)}\psi_{mn}(y,z)\times e^{-i\omega|x-x_j|/c_{mn}}, \quad (8a)$$

and

$$M(x,y,z|x_j)=\frac{\rho\omega h}{ab}\sum_{m,n}\sqrt{(2-\delta_{0m})(2-\delta_{0n})}(-1)^m\times\frac{\sin\left(\frac{m\pi h}{a}\right)\left[1-e^{-i\omega w/2c_{mn}}\cos\left(\frac{\omega x}{c_{mn}}\right)\right]}{i\left(\frac{m\pi h}{a}\right)(k^2-k_{mn}^2)}\times\psi_{mn}(y,z). \quad (8b)$$

The close forms of the double integrals in Eq. (7) are given in Appendix B. The corresponding force equation is[17]

$$F_j+F_{sj}+F_{mj}=\rho cwhV_jZ_j, \quad (9)$$

where Z_j is the acoustic impedance at the location of the jth piston seen by the wave propagating inside the duct. Suppose that there are N air pistons, then there will then be N simultaneous equations in the system

$$\begin{pmatrix} \alpha_{11} & \alpha_{12} & \cdots & \alpha_{1N} \\ \alpha_{21} & \alpha_{22} & \cdots & \alpha_{2N} \\ \vdots & \vdots & \ddots & \vdots \\ \alpha_{N1} & \alpha_{N2} & \cdots & \alpha_{NN} \end{pmatrix} \begin{pmatrix} V_1 \\ V_2 \\ \vdots \\ V_N \end{pmatrix} = \begin{pmatrix} F_1 \\ F_2 \\ \vdots \\ F_N \end{pmatrix}, \quad (10)$$

where the coefficients

$$\alpha_{ij} = \begin{cases} \rho c h w Z_j - \int_{-w/2}^{w/2} \int_{a-h}^{a} M(x,0,z|x_j)dzdx & \text{for } i = j, \\ -\int_{x_j-w/2}^{x_j+w/2} \int_{a-h}^{a} G(x,0,z|x_i)dzdx & \text{for } i \neq j. \end{cases} \quad (11)$$

It can be observed that $\alpha_{ij} = \alpha_{ji}$ for $i \neq j$. The solution of Eq. (10) is the vector $\mathbf{V} = [V_1, V_2, \ldots, V_N]$. The contribution of each dominant acoustic mode can then be estimated once $\mathbf{V}$ is found.

The acoustic impedance Z_j is resulted from the finite duct wall thickness, t, and the radiation impedance of the air piston Z_r. For simplicity, Z_j is assumed constant for a fixed frequency of excitation and it can be shown that

$$Z_j = \frac{Z_r - i\tan(kt)}{1 - iZ_r\tan(kt)}. \quad (12)$$

In the analytical part of this study, Z_r is obtained from Morse and Ingard[19] and, thus, is not explicitly shown here. Although this impedance is for a vibrating piston on an infinite rigid plan, its simplicity suffices, and the validity of this approximation will be tested by comparing the predictions of the above analytical model with the finite-element simulations. For demonstration purposes and simplicity, the square pistons are adopted in the foregoing analysis such that $h = w$ and $l = Nh$.

IV. RESULTS AND DISCUSSIONS

For the case of an infinitely long non-sound-leak rectangular duct, the results obtained from the FEM simulations and the above-presented semi-analytical calculations are very similar, even at frequencies close to the eigenfrequencies. The perfectly matched layers (PMLs) are, hence, working satisfactorily. The corresponding results are not presented. The foregoing discussions are focussed on the sound-leak duct cases. The sound fields are first analyzed using the FEM. Apart from revealing the physics of the sound propagation, these results will also provide the reference for testing the accuracy of the semi-analytical method discussed in Sec. III. A revised semi-analytical method is developed at the end of this section, and its predictions are compared with the finite-element simulations as well.

A. Small square openings

Figures 3(a) and 3(b) illustrate, respectively, the spectral variations of the sound power transmitted across and radiated out of the leaking sections with a single square opening located at $x/a = 1.76$ ($d = 1.76a$) with $t/a = 1/92$ obtained using the FEM. The transmitted sound powers W are calculated at the vertical plane just before the downstream PML using the standard formula,[20]

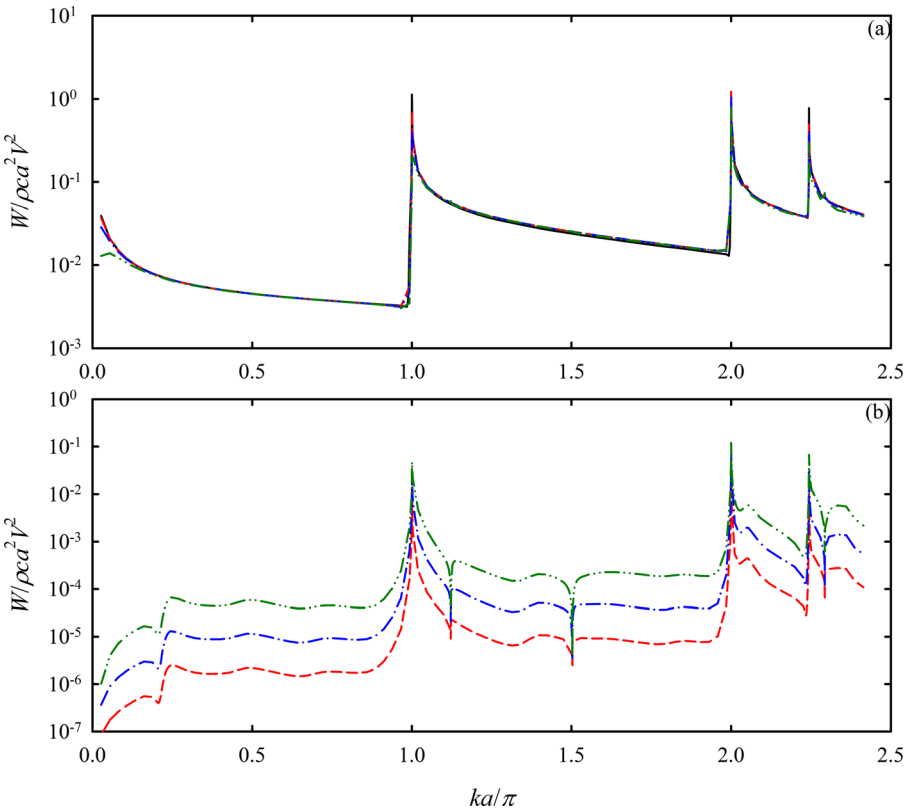

FIG. 3. (Color online) The spectral variations of the sound power transmitted across and radiated out of the sound-leak sections with a single square opening obtained using the FEM are shown. The (a) transmitted sound powers and (b) out-radiated sound powers are shown. —, Non-leaking duct; – – –, $h/a = 9/184$; —·—, $h/a = 9/92$; —··—, $h/a = 9/46$.

https://doi.org/10.1121/10.0007061

$$W = \frac{1}{4}\oint (pu^* + p^* u)\, dy\, dz, \tag{13}$$

where "*" denotes the complex conjugate and u is the complex acoustical particle velocity in the longitudinal direction. For the radiated power, the integration is performed on the outer surfaces surrounding the leaky section before the PMLs (Fig. 2). It is noted that the out-radiated powers are very weak compared to the transmitted powers in this single square opening case even at $h/a = 9/46$. The peak frequencies represent the eigenfrequencies of the leaky duct, which are identical to those of the corresponding rigid duct counterparts for $h/a \leq 9/46$ [Fig. 3(a)]. The square openings act like dampers. A similar observation has been made by Lin *et al.*,[8] although they focussed on the normal duct modes.

Strong sound leakage is found at the duct eigenfrequencies of the strong sound transmission because of the strong excitation of the acoustic modes [Fig. 3(b)]. Sharp narrowband drops of sound power, hereinafter referred as a "dip," which are not found in the non-leaking duct and the transmitted power spectra [Fig. 3(a)], are also observed at $ka/\pi \sim$ 1.12, 1.50, and 2.29. It is noted that the out-radiated sound power increases as the size of the opening increases.

Figure 4 illustrates the sound pressure magnitude distributions on the duct cross section where the opening is located at the peak and dip frequencies observed in Fig. 3 for $h/a = 9/46$. At $ka/\pi = 0.2441$, the sound pressure magnitude (as well as the real and imaginary parts) is relatively uniform across the duct cross section as shown in Fig. 4(a). This little peak in Fig. 3(b) is believed to be due to the Helmholtz resonator effect resulting from the opening and the duct cavity, but it does not give rise to a strong sound power flow along the duct. The peaks at $ka/\pi = 1$, 2, and 2.244 are caused by the strong excitation of the (1,0), (2,0), and (0,2) mode, respectively, as in the case of the rigid duct and, thus, are not discussed in detail. However, the corresponding modal patterns are slightly distorted to match the pressure-releasing condition at the small square opening [Figs. 4(b)–4(d)]. The dips in Fig. 3(b) are related to the asymmetric (0,1), (1,1), and (1,2) modes [Figs. 4(e)–4(g)], which are only excited in the presence of the asymmetric sound leakage. It should be noted that these modes are not excited by the sound source directly. Their strong excitations result from the piston-like air oscillations at the opening driven by the downstream propagating sound. These spanwise odd modes interact destructively with the strongly excited propagating (1,0), (2,0), and (0,2) modes, creating large quiet zones near to the opening and resulting in very weak sound radiation out of the duct cross section.

Modal analysis is performed to understand how the average sound power varies with the axial distance along the duct. As the closed forms of the leaky duct eigenmodes are not explicitly known, the eigenmode patterns of the straight rigid duct, ψ_{mn} [Eq. (2)], are used in this analysis. Because strong power flows can be found only near the eigenfrequencies, the foregoing discussions are mainly focussed on the sound propagation around these frequencies. The standard modal decomposition technique is used to estimate the magnitudes, A_{mn}, of the dominating acoustic modes. To do this, the cross section of the duct is discretized

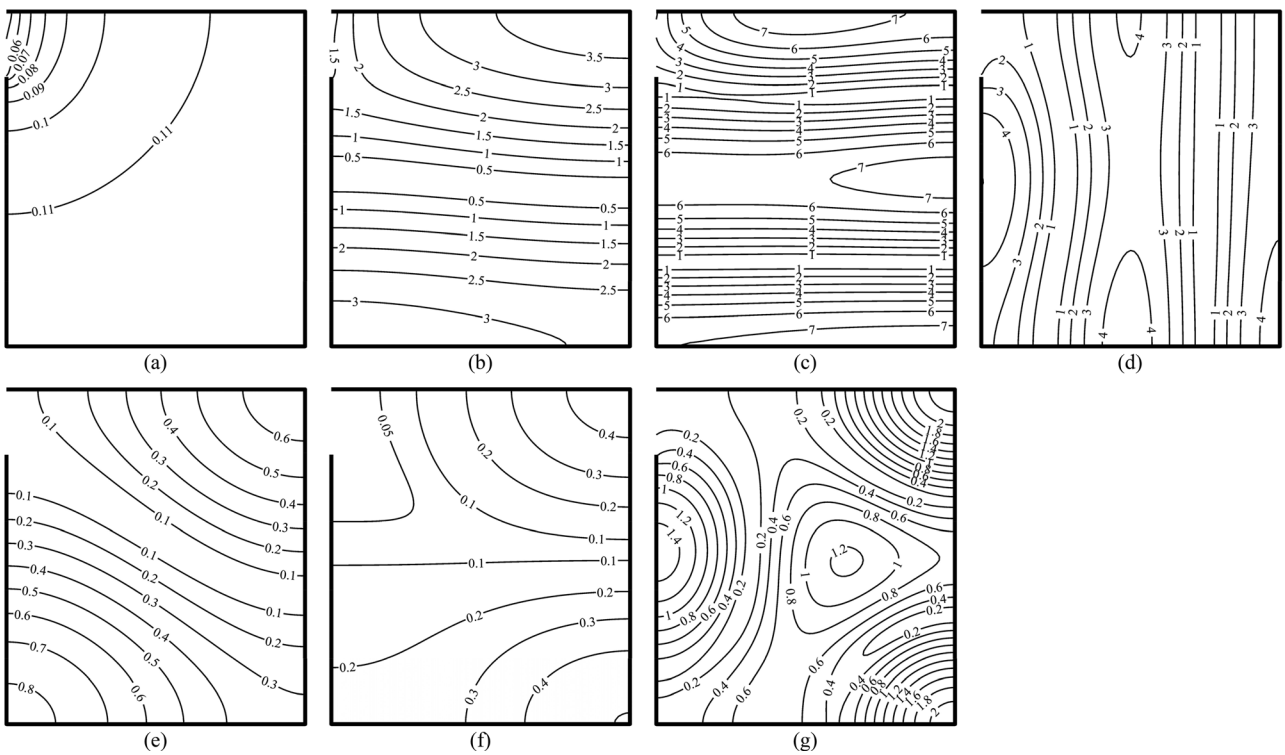

FIG. 4. The sound pressure magnitude distributions within the proximity of the square opening are shown. $h/a = 9/46$ and $x/a = 1.76$. (a) $ka/\pi = 0.244$; (b) $ka/\pi = 1.001$; (c) $ka/\pi = 2.000$; (d) $ka/\pi = 2.244$; (e) $ka/\pi = 1.122$; (f) $ka/\pi = 1.503$; and (g) $ka/\pi = 2.293$.

into a regular 46 (z) × 41 (y) gridding with a node separation of 2/92 in both the y- and z-directions,

$$A_{mn}(x) = \frac{1}{\Lambda_{mn}} \int_0^a \int_0^b p(x, y, z) \psi_{mn}(y, z)\, dy\, dz, \tag{14}$$

where Λ_{mn} is the norm of the modal function ψ_{mn}. For nodes next to the duct wall edge, their perpendicular distance from the nearest edge is 1/92.

Figure 5(a) shows the axial variations of the plane wave magnitudes $|A_{00}|$ computed by the FEM and the present semi-analytical method for $h/a = 9/46$. The shaded area denotes those locations directly under the sound source ($|x/R| < 1$) where Eq. (4) should be inapplicable. The corresponding data are, thus, not discussed, although the agreement between the FEM and semi-analytical method is good. The close agreement between the two sets of data for $|x/R| \geq 1$ (<1% difference) confirms that the simplified analytical approach has captured the essential features of the plane wave transmission across the leaky duct section. Similar or even better agreement is observed for smaller h/a and, therefore, the corresponding data are not presented.

The axial variations of the (1,0) mode magnitudes are presented in Fig. 5(b). Below the cut-on frequency, the mode exists in the form of an evanescent wave and its magnitude drops at an increased distance from the source as expected. The agreement of the results from the two approaches is very good. Such an agreement is less satisfactory only at a frequency very close to the eigenfrequency of the (1,0) mode, but the discrepancy is just 3%–4%. A similar level of agreement is again observed for the (2,0) mode near its eigenfrequency as shown in Fig. 5(c). One can also observe that there is a chance for the magnitude of (2,0) mode downstream of the sound leaking opening to be higher than that of its upstream counterpart when the excitation frequency gets further away from the (2,0) mode eigenfrequency.

The abovementioned discrepancy becomes worse as the excitation frequency is further increased to $ka/\pi \sim 2.2$ [Fig. 5(d)]. One can observe that there is a misalignment between the mode magnitude axial variation patterns predicted by the two approaches. The situation is much better for the smaller opening size of $h/a \leq 9/92$ (not shown here), suggesting that the wavelength of the exciting sound relative to the opening dimension is a crucial parameter. A correction to the semi-analytical approach for non-compactness will be necessary. It will be discussed in detail in Sec. IV B.

One can also observe from Fig. 5(d) that the downstream (0,2) mode magnitude becomes higher than that at the upstream mode magnitude at a frequency closer to the eigenfrequency of the dominant (0,2) mode than in the case

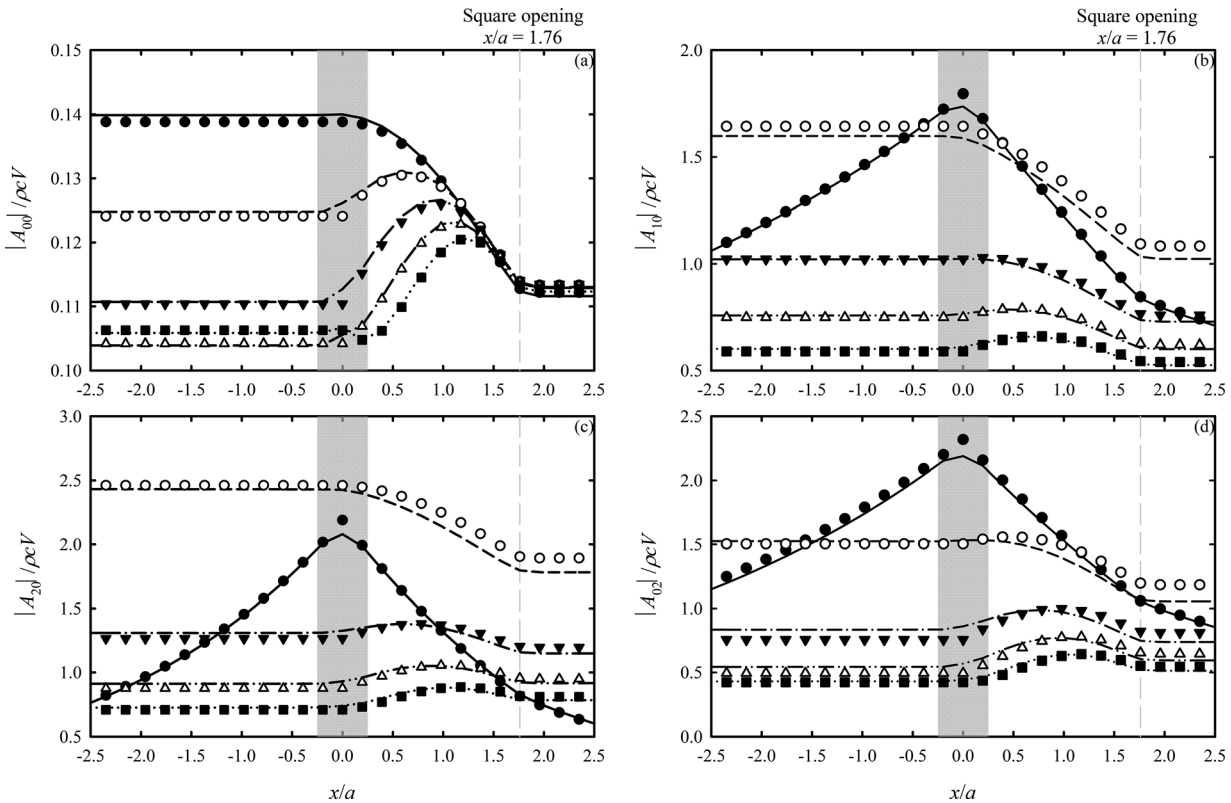

FIG. 5. The axial variations of the acoustic mode magnitudes for $h/a = 9/46$ are shown. The square opening at $x/a = 1.76$. (a) (0,0) mode; semi-analytical method: ●, $ka/\pi = 0.161$; ○, $ka/\pi = 0.241$; ▼, $ka/\pi = 0.322$; △, $ka/\pi = 0.402$; ■, $ka/\pi = 0.483$. FEM: ——, $ka/\pi = 0.161$; – – –, $ka/\pi = 0.241$; —·—, $ka/\pi = 0.322$; —··—, $ka/\pi = 0.402$; · · ·, $ka/\pi = 0.483$. (b) (1,0) mode; semi-analytical method: ●, $ka/\pi = 0.998$; ○, $ka/\pi = 1.009$; ▼, $ka/\pi = 1.019$; △, $ka/\pi = 1.030$; ■, $ka/\pi = 1.041$; FEM: ——, $ka/\pi = 0.998$; – – –, $ka/\pi = 1.009$; —·—, $ka/\pi = 1.019$; —··—, $ka/\pi = 1.030$; · · ·, $ka/\pi = 1.041$. (c) (2,0) mode, semi-analytical method: ●, $ka/\pi = 1.996$; ○, $ka/\pi = 2.006$; ▼, $ka/\pi = 2.017$; △, $ka/\pi = 2.028$; ■, $ka/\pi = 2.039$. FEM: ——, $ka/\pi = 1.996$; – – –, $ka/\pi = 2.006$; —·—, $ka/\pi = 2.017$; —··—, $ka/\pi = 2.028$; · · ·, $ka/\pi = 2.039$. (d) (0,2) mode, semi-analytical method: ●, $ka/\pi = 2.242$; ○, $ka/\pi = 2.253$; ▼, $ka/\pi = 2.263$; △, $ka/\pi = 2.275$; ■, $ka/\pi = 2.285$. FEM: ——, $ka/\pi = 2.242$; – – –, $ka/\pi = 2.253$; —·—, $ka/\pi = 2.263$; —··—, $ka/\pi = 2.275$; · · ·, $ka/\pi = 2.285$.

https://doi.org/10.1121/10.0007061

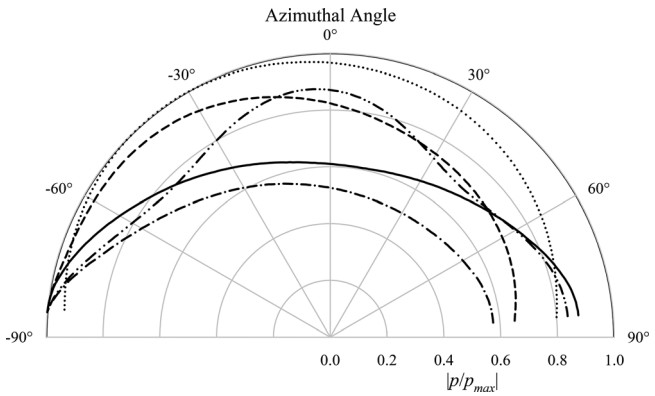

FIG. 6. The directivity of the sound radiation out of a non-compact slot is shown. · · ·, $h/a = 9/184$, $l/h = 1$, $ka/\pi = 1.000$; ——, $h/a = 9/184$, $l/h = 10$, $ka/\pi = 1.000$; – – –, $h/a = 9/184$, $l/h = 10$, $ka/\pi = 2.000$; —·—, $h/a = 9/92$, $l/h = 5$, $ka/\pi = 1.000$; —··—, $h/a = 9/92$, $l/h = 5$, $ka/\pi = 2.244$.

of the (2,0) mode. It is believed that the same should take place around the (1,0) mode eigenfrequency, but the magnitude of that mode should be insignificant as the corresponding frequency should be quite far above the (1,0) mode eigenfrequency.

B. Non-compact slots

As the slot becomes long relative to the wavelength of the excitation sound, the acoustical particle velocities within the slot will become less uniform, and the sound field outside the slot deviates from the monopole as shown in Fig. 6, where the azimuthal angle of 0° represents the radiation normal to the slot. The negative azimuthal angle denotes the backward radiation. One can notice that the sound field is already not symmetrical for the square opening of $h/a = 9/184$, but the asymmetry is small such that the assumption of normal sound radiation out of that short slot in Sec. III can still work satisfactorily. As the length of the slot increases, the accumulative effect of such a small asymmetry along the length of the slot results in significant error in the model presented in Sec. III. For $l/a = 45/92$, one can see very asymmetrical radiation patterns near all of the important duct eigenfrequencies. However, there appears no definite trend for the variation of the radiation directivity with the frequency or slot size.

Figure 7 illustrates the pressure distributions along the duct obtained by the FEM near the three lower order acoustic modes for $h/a = 9/184$, $l/a = 180/92$. The cases of the longest slot are chosen to better illustrate the modal development under the influence of the sound leakage. One can observe that individual acoustic modes are strongly excited and propagating upstream of the sound source for all of the cases presented. For $ka/\pi = 1.000$ and a narrow slot width of $h/a = 9/184$, one can notice the weakly excited (0,1) mode at $x/a = 1.5$, which is a location between the loudspeaker and the slot [Fig. 7(a)(ii)]. However, this mode is evanescent and, thus, is insignificant upstream. In the middle of the sound leaking region at $x/a = 2.71$ [Fig. 7(a)(iii)], the sound leakage gives rise to the evanescent (0,1) mode, but the strong (1,0) mode remains intact. The (1,0) mode remains

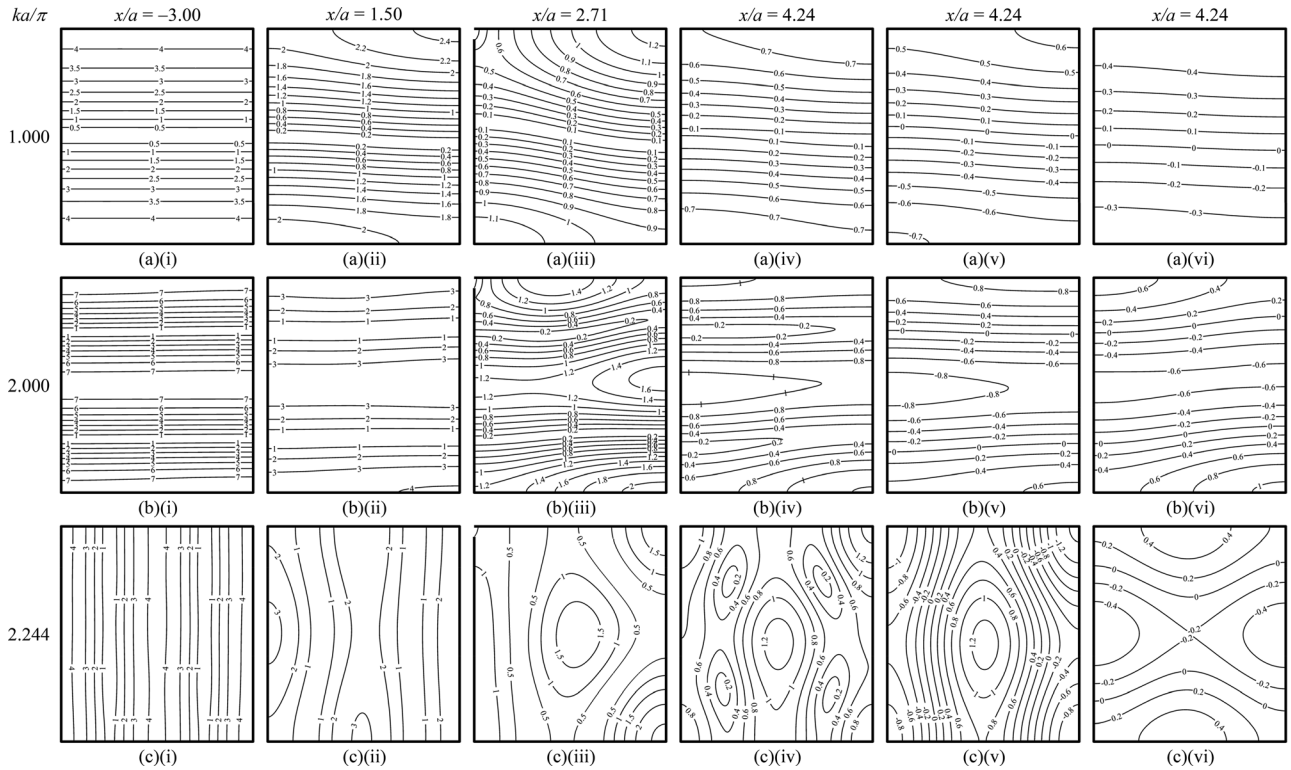

FIG. 7. The acoustic mode development along the duct and sound pressure magnitude ($|p|/\rho cV$) distributions for $h/a = 9/184$, $l/a = 180/92$ is shown. (a) $ka/\pi = 1.000$; (b) $ka/\pi = 2.000$; (c) $ka/\pi = 2.244$; (i) $x/a = -3.00$; (ii) $x/a = 1.50$; (iii) $x/a = 2.71$ (middle of slot); (iv) $x/a = 4.24$; (v) $x/a = 4.24$, $\mathrm{Re}(p/\rho cV)$; and (vi) $x/a = 4.24$, $\mathrm{Im}(p/\rho cV)$.

dominant downstream of the slot at $x/a = 4.24$ as shown in Fig. 7(a)(iv). In Figs. 7(a)(v) and 7(a)(vi), the real and imaginary parts of the pressure distribution at $x/a = 4.24$ are presented [hereinafter denoted as Re(p) and Im(p), respectively]. Whereas one can note the strong (1,0) mode and weak (0,1) mode in Re(p), the asymmetrical vertical distribution of Im(p) manifests the existence of the planar mode. However, the (1,0) mode substantially dominates the overall sound field downstream of the sound-leak section, although its magnitude has been largely reduced because of the slot opening.

The situations for $ka/\pi = 2.000$ are very similar to those for $ka/\pi = 1.000$ as shown in Fig. 7(b), except that the dominant mode in this case is the (2,0) mode. One can notice the existence of the weakly propagating $n = 1$ modes [(0,1) and (1,1)] downstream of the sound source [Figs. 7(b)(v) and 7(b)(vi)]. However, the presence of a planar mode is not obvious. Again, the (2,0) mode is substantially weakened due to the sound leaking slot, but it is still dominating the overall sound field, although the asymmetrical spanwise $n = 1$ modes are stronger than those for $ka/\pi = 1.000$ as they are no longer evanescent.

Figure 7(c) illustrates the development of the sound field in the duct when the symmetrical spanwise (0,2) mode is strongly excited. Leakage of the (0,2) mode sound energy is significant. Downstream of the slot at $x/a = 4.24$, there is clear evidence on the co-existence of the (2,0) and (0,2) modes. Their magnitudes are comparable. One can observe from the patterns of Re(p) and Im(p) [Figs. 7(c)(v) and 7(c)(vi)] that the (0,2) mode is slightly stronger. Both of these patterns are basically of the form

$$A\cos(2\pi z/a) + B\cos(2\pi y/b), \tag{15}$$

with $|A| > |B|$.

Figure 8 quantitatively summarizes the modal developments shown in Fig. 7. One can see the decay of evanescent modes as they propagate away from the sound-leak section.

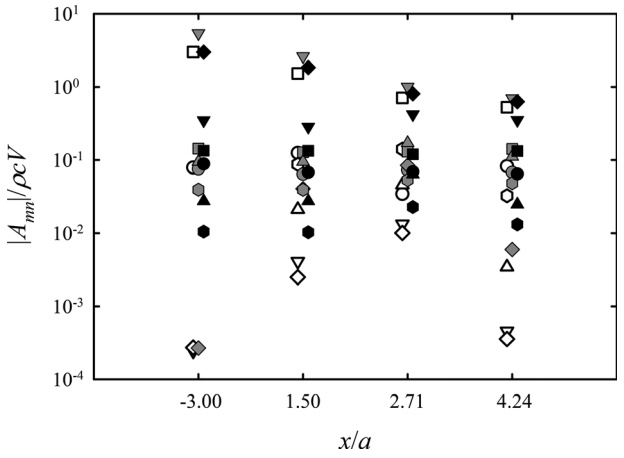

FIG. 8. The acoustic mode magnitude variation along the duct for $h/a = 9/184$ and $l/a = 180/92$ is shown. ●, (0,0) mode; ■: (1,0) mode; ⬢, (0,1) mode; ▲, (1,1) mode; ▼, (2,0) mode; ◆, (0,2) mode. Open symbol, $ka/\pi = 1.000$; gray, $ka/\pi = 2.000$; and black, $ka/\pi = 2.244$.

Also, the co-dominance of the (2,0) and (0,2) modes of similar magnitude for $x/a \geq 2.71$ at $ka/\pi = 2.24$ is confirmed. In fact, a large variation of the mode magnitude can only be found at frequencies close to the three relatively more important acoustic modes shown in Fig. 3 (that is, $ka/\pi = 1$, $ka/\pi = 2$, and $ka/\pi = 2.244$). Away from each of these frequencies, the magnitudes of the other modes forced out at that particular frequency do not vary much with the frequency and longitudinal location along the duct provided that they are not evanescent. The magnitudes of the acoustic modes with $n = 1$ are, in general, weak as the symmetrical sound source in this study does not create such modes directly.

In Fig. 9, the acoustic mode developments for the case of a wide slot with $h/a = 9/46$ are presented. The situations for $ka/\pi = 1.000$ and 2.000 are very similar to those for $h/a = 9/184$ [Figs. 7(a) and 7(b)], except that there are slightly stronger $n = 1$ modes in this case. The wider slot results in greater sound leakage and, hence, stronger excitation of these modes regardless of whether they are evanescent or propagating. Therefore, the corresponding results are not further discussed. The symmetrical spanwise (0,2) mode is again strongly weakened. However, similar to the case for the narrow slot [Fig. 7(c)], this mode no longer dominates the overall sound field downstream of the slot as shown in Figs. 9(c)(iv)–9(c)(vi). The signatures of the (2,0) and (0,2) modes can be found in Re(p) at $x/a = 4.24$, where the Re(p) distribution pattern can be represented by Eq. (15). However, it is clearly seen that the (2,0) mode dominates the Im(p). In addition, a weak signature of $n = 1$ modes can be found in Figs. 9(c)(iv)–9(c)(vi).

The corresponding variations of the modal magnitudes with the frequency and axial location along the duct for $h/a = 9/46$, $l/a = 180/92$ are shown in Fig. 10. For a larger h/a, the leaking of the sound energy close to the three relatively important lower order acoustic modes is stronger. For $ka/\pi = 2.244$, the magnitudes of the (0,0), (1,0), (2,0), and (0,2) downstream of the slot are quite similar with a difference within one order of magnitude. Because the results are very similar to those discussed in Fig. 8 for the case of $h/a = 9/184$, $l/a = 180/92$. They are not discussed further. The reduction of l/a will only increase the modal magnitudes without much effect on the modal development and, thus, the corresponding results are not presented.

The sharpness of the acoustic mode excitation is reduced as the slot length increases as shown in Fig. 11. It is rather expected as the increased sound leakage area is seen by the sound as an increase in the damping of its transmission across the sound-leak duct section. The same happens when the slot width is increased at a fixed slot length as can be seen from the data of $h/a = 9/46$, $l/h = 10$, also shown in Fig. 11. The main characteristics of the data with $h/a = 9/92$ are very similar to those presented in Fig. 11 and, therefore, they are not presented here. One can also notice that there are multiple weak/blurred peaks near the (2,0) and (0,2) eigenfrequencies of the corresponding non-leaky duct. However, the magnitudes of the peaks near the latter are

https://doi.org/10.1121/10.0007061

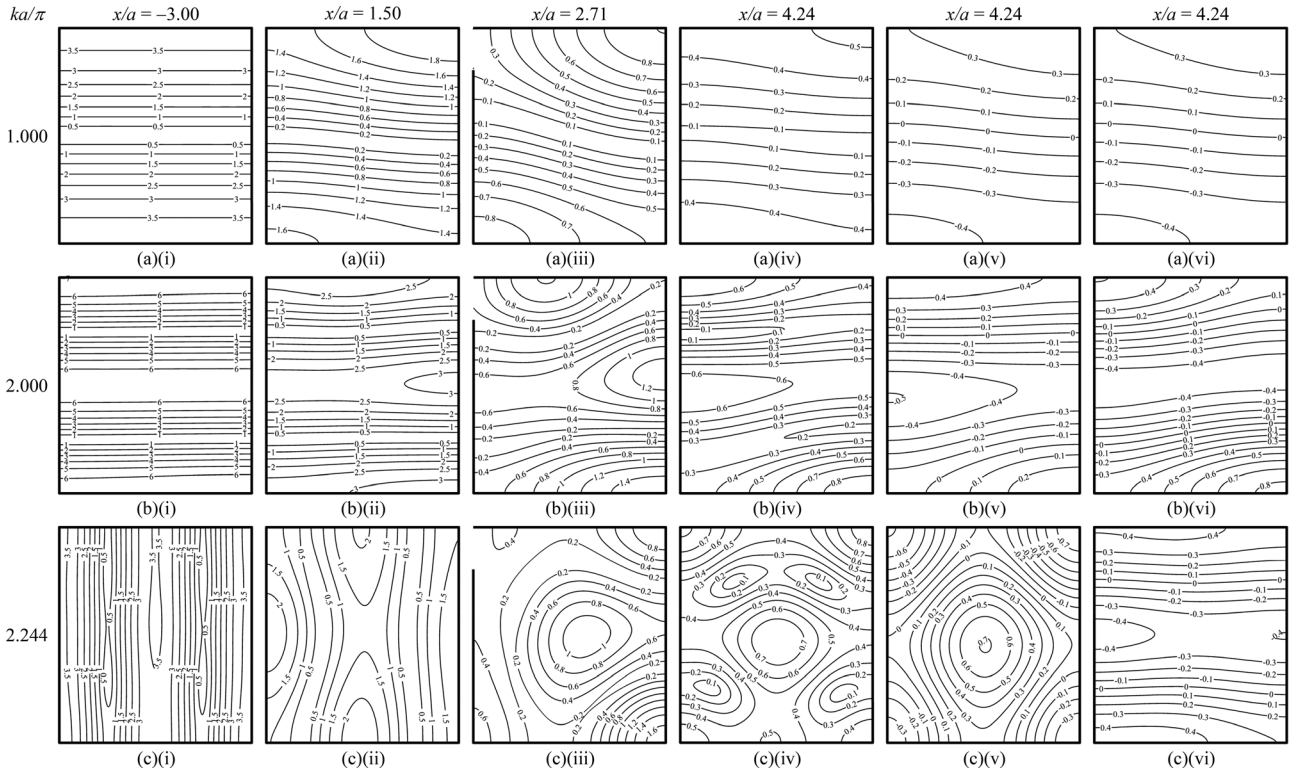

FIG. 9. The acoustic mode development along the duct and sound pressure magnitude ($|p|/\rho cV$) distributions for $h/a = 9/46$ and $l/a = 180/92$ is shown. The legends are the same as those in Fig. 7.

comparable. The acoustic impedance of the opening is believed to play a key role in the shift of the peak frequencies when the opening is large. It is left to further investigation.

Figure 12 summarizes the effects of the slot length and width on the peak sound power transmission frequencies and transmitted power magnitudes. For the transverse modes, the frequency of the major transmitted power peak tends to increase with l/h and/or h/a, but its magnitude decreases at the same time. The number of minor sound power peaks increases as the frequency, slot width, and/or slot length increase as well. For $h/a = 9/46$, the magnitudes of these peaks are comparable to those of the major peaks for the slot cases. For the spanwise (0,2) mode [see Fig. 12(c)], the major peak frequency does not depend on the slot width or slot length unless the slot width is large. Again, the minor peak magnitudes become similar to those of the major peak when the slot length is long or when the slot width is relatively wide.

Eventually, the semi-analytical approach described in Sec. III cannot capture the characteristics of the particle

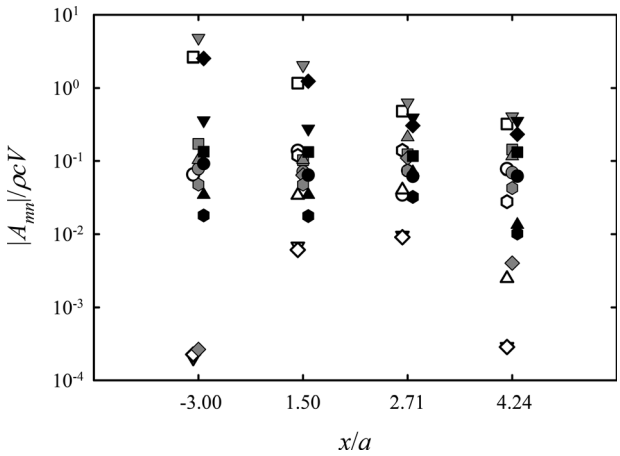

FIG. 10. The acoustic mode magnitude variation along the duct for $h/a = 9/92$ and $l/a = 180/92$ is shown. The legends are the same as those in Fig. 8.

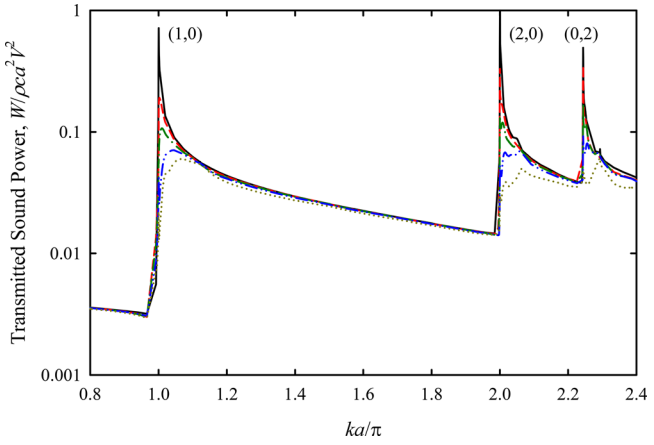

FIG. 11. (Color online) The examples of the transmitted sound power spectra of the non-compact slots are shown. —, $h/a = 9/184$, $l/h = 1$; – – –, $h/a = 9/184$, $l/h = 10$; -·-, $h/a = 9/184$, $l/h = 20$; -···-, $h/a = 9/184$, $l/h = 40$; and · · ·, $h/a = 9/46$, $l/h = 10$.

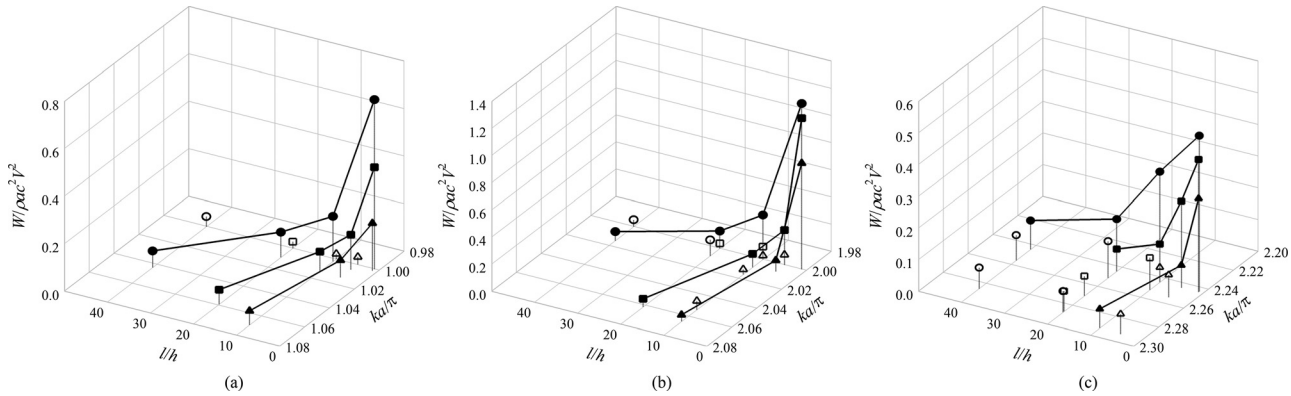

FIG. 12. The spectral peaks of the transmitted sound power of the non-compact slots are shown. (a) Near (1,0) mode; (b) near (2,0) mode; and (c) near (0,2) mode; closed symbols, major peak; open symbols, minor peaks; ●, $h/a = 9/184$; ■, $h/a = 9/92$; and ▲, $h/a = 9/46$.

velocity variation along the slot, and fails to predict the axial variations of the sound power (not shown here). Refinement of the model is necessary for the non-compact slots.

One can always consider the particle velocity variation along the slot as an infinite series of eigenmodes of unknown magnitudes by treating the slot of thickness t as a thin rectangular cavity.[21] Mode matching may then be adopted to solve the problem in principle.[6,10] However, this approach is very complicated as well as tedious. The most important sound power transmission takes place near the eigenfrequencies, and the corresponding wavelength of the longitudinal propagating wave along the slot is very long compared to the slot length.

For simplicity, we assume that the longitudinal variations of the transverse particle velocity along the length of the sound leaking slot opening, $v(x')$, at a frequency near an eigenfrequency takes the form of a propagating wave as shown in Fig. 13,

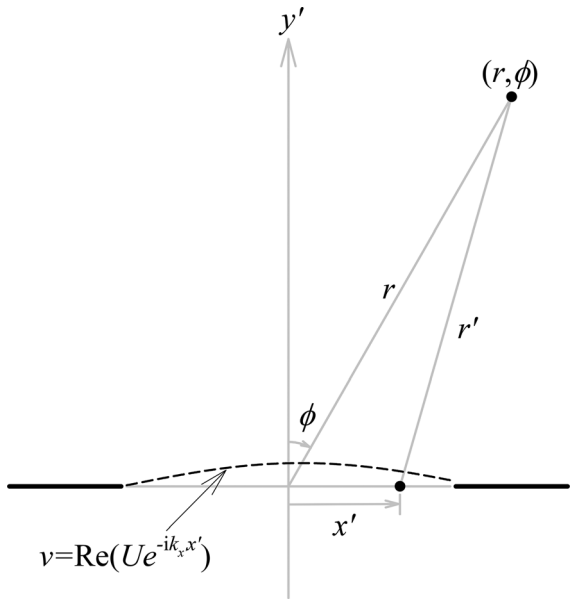

FIG. 13. The schematics of the proposed model of the sound radiation out of an opening are shown.

$$v(x') = Ue^{-ik_{x'}x'}, \tag{16}$$

where U is an unknown magnitude and $k_{x'}$ is the complex wavenumber, which is also unknown. The sound that is radiated out from the opening (assume to be baffled for simplicity) in the far field is[22]

$$\begin{aligned} p(r,\phi) &= \int_{-l/2}^{l/2} \frac{i\rho\omega hU}{2\pi r'} e^{-ik_{x'}x'} e^{-kr'} dx' \\ &= \frac{i\rho\omega hU}{\pi r} e^{-kr} \frac{\sin\left(\frac{1}{2}kl\sin\phi - \frac{k_{x'}}{2}l\right)}{kl\sin\phi - k_{x'}l}. \end{aligned} \tag{17}$$

One can observe that for small $|k_{x'}l|$, which is the case at the frequencies close to a duct mode eigenfrequency in the presence of a small slot opening, the radiation should be monopole-like but with a very weak directivity at the angle ϕ relative to the central plane of the small slot opening, where

$$\sin\phi = \frac{k_{x'}}{k}. \tag{18}$$

Sound is not radiated in a direction normal to the slot as assumed previously in Sec. III and Fig. 6. The transverse component of the wavenumber of the sound radiation is

$$k_{y'} = k\cos\phi = k\sqrt{1-(k_{x'}/k)^2}. \tag{19}$$

It is proposed to estimate the sound propagation across the sound-leak section of the duct by replacing k in Eqs. (5), (6), and (12) by an expression similar to that of $k_{y'}$, shown in Eq. (19), when the slot is no longer compact.

In the present study, the component of k relevant to the sound radiation out of the slot is k_y. The component of k within the slot is, thus, $\sqrt{k^2-k_y^2}$. However, the above simplified approach does not yield the analytical close form solution for this wavenumber component. Denoting within the slot,

$$\frac{\sqrt{k^2-k_y^2}}{k} = \varepsilon e^{i\gamma} = D, \tag{20}$$

https://doi.org/10.1121/10.0007061

where ε is a very small positive real number and γ is the phase angle such that $k_y = k\sqrt{1-D^2}$, the target hereinafter is to develop a framework to estimate ε and γ, which will result in minimum deviation between the FEM predictions and those estimated using the modified Eqs. (5), (6), and (12) (hereinafter referred to as the modified modal approach). In this study, this deviation Δ is defined as

$$\Delta = \sqrt{\frac{1}{V_d}\oint\left(\frac{|p_{\mathrm{FEM}}| - |p_{\mathrm{mode}}|}{|p_{\mathrm{FEM}}|}\right)^2 dV_d}, \tag{21}$$

where the integration is performed over the main computation duct volume V_d in the present study, and the subscripts "FEM" and "mode" denote predictions by the FEM and modified modal equations, respectively. Δ is a function of D. The root of the differential equation $d\Delta/dD = 0$, therefore, gives the optimal combination of ε and γ. It can be found using Newton's method with the complex variable D. The required derivatives are estimated numerically with the intervals $\Delta\varepsilon$ and $\Delta\gamma$ set at 10^{-5} and $10^{-5}\pi$, respectively. This spacing is small enough to cater for the highest frequency of interest in the present study.

Figure 14 summarizes the variation of ε and γ with the slot dimension near the three lower order important duct eigenfrequencies. One can see that the phase angle γ does not vary much for a fixed slot dimension, and it decreases as the frequency increases, in general. The magnitude ε increases as the frequency increases for a fixed slot dimension. The wavelength of the major propagating wave inside the duct just after the cut-on of the higher mode is very long such that the excitation along the slot is more uniform and, thus, ε is small. Although ε increases as the frequency increases away from an eigenfrequency, the magnitude of the transmitted power decreases quickly at the same time (Fig. 5). One can also notice that ε decreases with the increasing slot length. It becomes very weak near the eigenfrequencies of the (0,2) and (2,0) duct modes. For longer slots at a higher frequency, the interference from the different parts of the slot wave results in less directional sound radiation into the far field overall. Similar phenomenon can be found in the vibro-acoustics of plates and shells.[23] Besides, it appears that ε is not so dependent on the slot width h.

Figure 15 illustrates some examples of the axial variations of the acoustic mode magnitudes along the duct estimated using the optimized Ds. The agreements between the FEM results and revised modal equation predictions are much better than those obtained without D. The modified modal approach gives a very good prediction of A_{mn}, and the percentage deviation between the FEM results and predictions using D ranges between 0.03% and 4.11% with a root mean square (RMS) value of 1.27% for the cases included in the present study. Table II summarizes the RMS deviations between the predictions obtained by using D and the FEM. The deviations are relatively larger for long and/or wide slots near the eigenfrequency of the (2,0) mode. This is the condition at which the variation of the acoustical particle velocity along the width of the slot is relatively less uniform. For the widest slot included in the present study, the deviations at the frequencies near the eigenfrequency of the (0,2) mode are also relatively large, probably for the same reason.

C. Empirical prediction framework for *D*

It is obvious that ε is related to the wavenumber of the propagating component $\sqrt{k^2 - k_{mn}^2}$, k, l, h, and a. One can derive several dimensionless parameters for this ε family, but for simplicity, the number of such parameters is kept to three in this study. We choose the form

$$\varepsilon = f\left(\frac{\sqrt{k^2 - k_{mn}^2}}{k}, \frac{l}{a}, \frac{h}{a}\right). \tag{22}$$

Assuming that a power law exists between ε and the three dimensionless parameters in Eq. (22), using the method of least square and the data shown in Fig. 14, one obtains the following approximation for ε:

$$\varepsilon = 1.02422\left(\frac{\sqrt{k^2 - k_{mn}^2}}{k}\right)^{1.30873}\left(\frac{l}{a}\right)^{-0.38283}\left(\frac{h}{a}\right)^{-0.03033}, \tag{23}$$

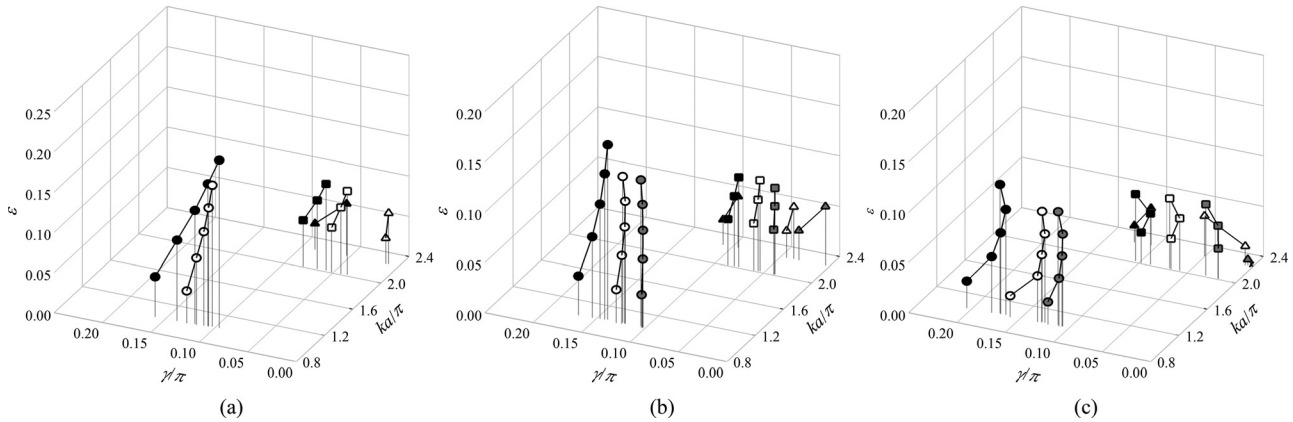

FIG. 14. The variations of D with the frequency and slot dimensions are shown. (a) $l/a = 45/92$; (b) $l/a = 90/92$; (c) $l/a = 180/92$; ●, $ka \sim \pi$; ■, $ka \sim 2\pi$; ▲, $ka \sim 2.24\pi$; solid symbol, $h/a = 9/184$; open symbol, $h/a = 9/92$; and gray symbol, $h/a = 9/46$.

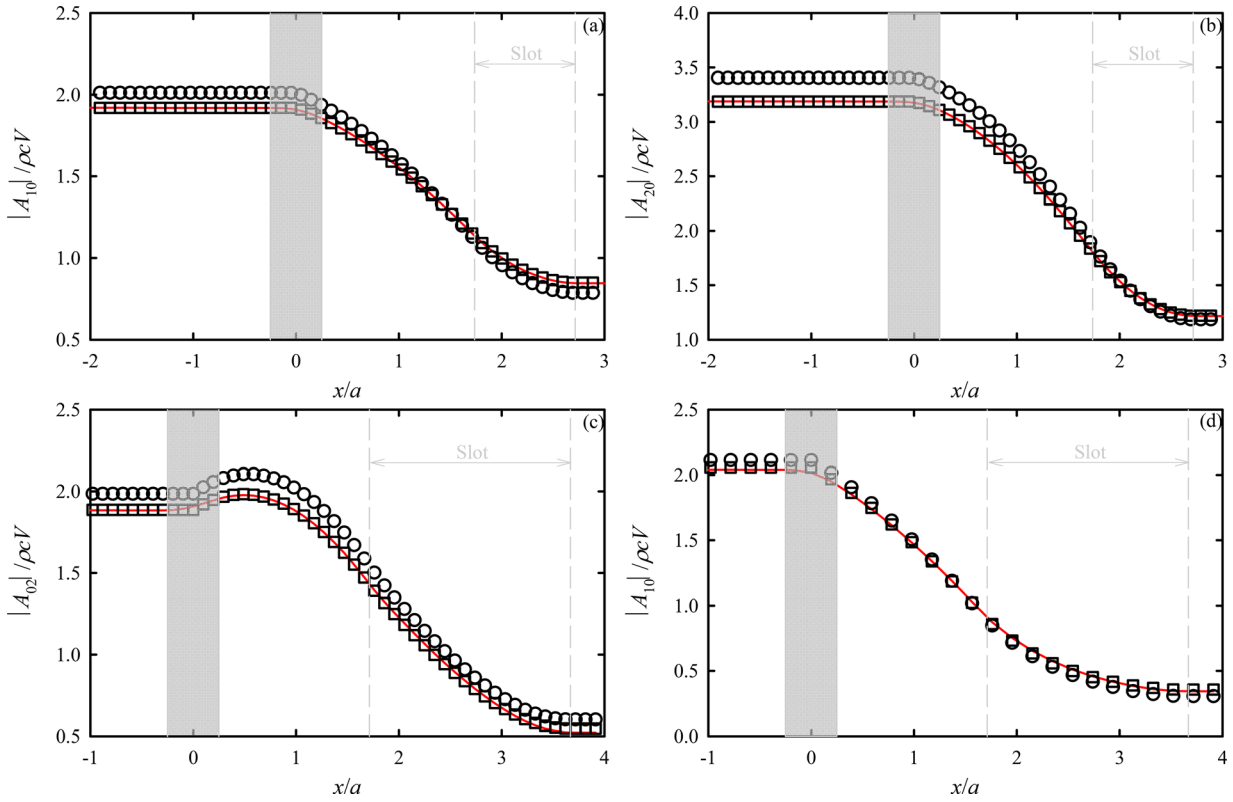

FIG. 15. (Color online) The examples of the axial variations of the acoustic mode magnitudes predicted using D are shown. (a) $h/a = 9/184$, $l/a = 45/92$, $ka = 1.009\pi$; (b) $h/a = 9/184$, $l/a = 90/92$, $ka = 2.006\pi$; (c) $h/a = 9/92$, $l/a = 180/92$, $ka = 2.253\pi$; and (d) $h/a = 18/92$, $l/a = 180/92$, $ka = 1.009\pi$; —, FEM; ○, without D ($D = 0$); □, with D.

where a correlation coefficient R^2 is 0.9622 and a RMS deviation is 0.0083. The weak dependency of ε on h/a is further manifested.

One can do the same least square regression for γ. However, one can see from Fig. 12 that the phase γ does not basically scale with $\sqrt{k^2 - k_{mn}^2}$. In fact, the inclusion of this parameter or its derivatives into the regression model will result in a very poor fitting (not shown here). It is clear that γ tends to decrease with ka. Through regression, one obtains

$$\frac{\gamma}{\pi} = 2.13924(ka)^{-0.04997}\left(\frac{l}{a}\right)^{0.00954}\left(\frac{h}{a}\right)^{-0.02195} - 2, \qquad (24)$$

and the corresponding correlation coefficient and RMS deviation are 0.8957 and 0.0153, respectively. Figure 16 concludes the performance of the present prediction framework for D. The maximum percentage deviation of the corresponding prediction from the FEM simulation is 6.16% with a RMS value of 2.42%. A comparison between the performance of the predicted D [Eqs. (23) and (24)] and the optimized D obtained using Newton's method is given in Table II. The higher Δs resulted from the predicted D is not surprising. However, the deviations are still well within the engineering tolerance. Again, the deviation is, in general, larger for longer and/or wider slots at a frequency near that of the (2,0) mode. The largest deviation is observed for the longest and widest slot near the (0,2) mode.

Calculations with some new slot configurations and a different duct cross section aspect ratio are performed to test the applicability of Eqs. (23) and (24). As the spans of the related duct-like structures, in practice, can be longer than their widths ($b/a > 1$), the foregoing duct section is chosen to have an aspect ratio of $b/a = 134/56 = 2.39$. In fact, the structures with $b/a > 2.5$ are less commonly found in practice. As Δ is usually larger for a longer slot and/or larger slot width, the slot length in the foregoing analysis is fixed at $\sim 2a$ and the largest slot width is kept at $\sim 20\%$ of a as in the above analysis. For such a duct cross section, the three lower order important eigenmodes are the (1,0), (0,2) and (1,2) modes. Again, the (0,1) mode is only very weakly excited because of the symmetrical wall-mounted circular sound source. The corresponding Δs are tabulated in Table III. One can observe that the deviations are comparable to those presented in Table II, although Eqs. (23) and (24), which are developed based on the previous duct data, are used for predicting D. This tends to suggest that these equations are useful within the duct cross section aspect ratio range of the present study.

V. CONCLUSIONS

The acoustic mode propagation along an infinite rigid duct-like structure with a finite length sound-leak section is investigated using the method of finite elements in the present study. The sound leaking section consists of a small opening or a slot fixed at a corner of the duct-like structure. Effort is also made on the development of a simplified framework with the use of the modal solutions of the wave

https://doi.org/10.1121/10.0007061

TABLE II. The derivations of the predictions from the finite-element simulations.

			RMS Δ (%)	
h/*a*	*l*/*h*	Mode	Newton's method	Eqs. (23) and (24)
9/184	10	(1,0)	0.115	0.707
		(2,0)	0.225	0.659
		(0,2)	0.234	0.704
	20	(1,0)	0.157	0.869
		(2,0)	0.276	1.371
		(0,2)	0.393	1.130
	40	(1,0)	0.959	1.583
		(2,0)	1.844	2.365
		(0,2)	0.491	1.102
9/92	5	(1,0)	0.145	1.552
		(2,0)	0.241	0.798
		(0,2)	0.263	0.710
	10	(1,0)	0.204	1.404
		(2,0)	0.285	2.503
		(0,2)	0.399	0.714
	20	(1,0)	1.191	3.869
		(2,0)	3.241	4.104
		(0,2)	1.167	2.370
9/46	5	(1,0)	0.298	1.279
		(2,0)	0.594	2.555
		(0,2)	0.910	3.582
	10	(1,0)	1.635	3.275
		(2,0)	3.244	4.245
		(0,2)	3.383	5.577

TABLE III. The deviations of the predictions from the finite-element simulations for the duct with a cross-section aspect ratio of 2.39:1 (134:56).

h/*a*	*l*/*h*	Mode	RMS Δ by Eqs. (23) and (24) (%)
6/56	20	(0,2)	3.262
		(1,0)	2.651
		(1,2)	1.858
12/56	10	(0,2)	4.033
		(1,0)	3.459
		(1,2)	4.791

equation for modelling the sound propagation inside the duct near the rigid duct eigenmode frequencies at which the strong sound power propagation results. In the present study, the slot height is capped at ∼20% of the duct height and its maximum length is 1.95 times the duct height.

The results of the finite-element simulation show that many different modes are generated through the interactions between the sound source and sound leaking slot. However, the odd spanwise modes remain relatively weak even they are not evanescent. Significant sound power propagation is only observed at frequencies close to the eigenfrequencies of the rigid duct. However, the strengths of the transverse acoustic modes and the plane wave mode downstream of the sound-leak section become more comparable as the slot widths and/or lengths increase. The sound field upstream of the sound-leak section is dominated by the mode having an eigenfrequency close to the excitation frequency, whereas the magnitudes of the other modes, provided that they are not evanescent, are fairly constant along the whole duct.

The analytical modal solution of the wave equation inside the duct with a square opening at the duct corner is first determined by assuming a uniform normal acoustical particle velocity across the opening. Each slot involved in the present study is modelled as an array of identical pistons. The corresponding solution for the sound propagation is then estimated based on the square opening solutions and mutual interactions between the pistons that form the slot. For the square opening cases, the abovementioned relatively standard modal approach is found able to produce results which agree satisfactorily with the finite-element simulations.

However, the above normal uniform particle velocity assumption is found inapplicable for the slots. By considering such a velocity as a spatially growing propagating wave

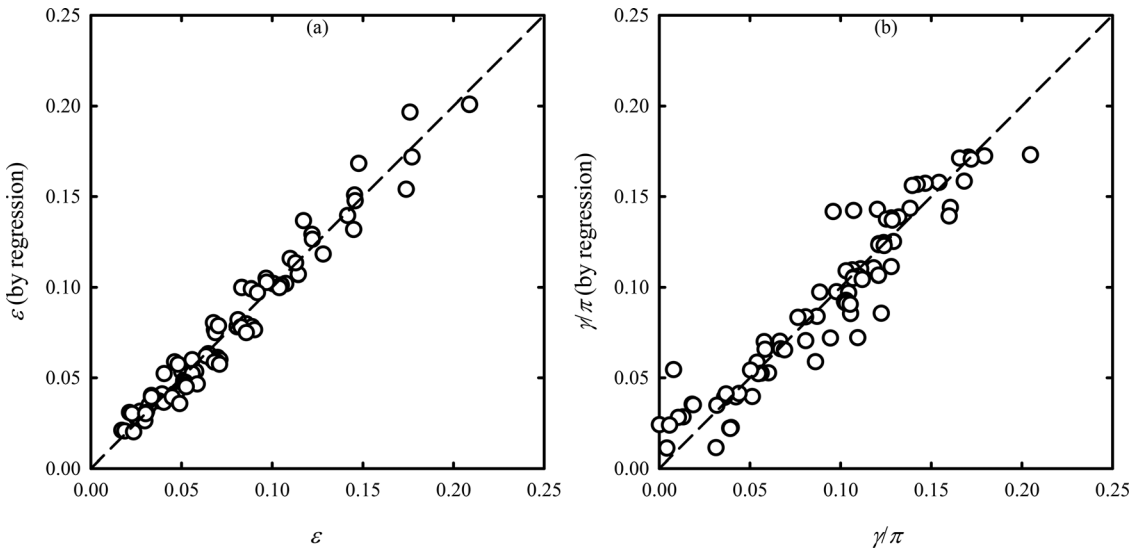

FIG. 16. The prediction of D by the multivariate regression [Eqs. (23) and (24)]. (a) ε and (b) γ/π are shown. – – –, Line of equality.

across the opening, it is found that the major sound radiation axis makes an oblique angle with the opening normal, and this is confirmed by finite-element simulation. The propagation wavenumber can then be related to the excitation sound wavenumber by a complex ratio, which varies with the excitation frequency, a duct mode, as well as slot dimensions. The modal solution is then revised to include this ratio. The analytical determination of this ratio is too complicated. In this study, this ratio is optimized by Newton's method using the finite-element simulations as the reference. The agreement between the finite-element simulations and revised modal approach is well within the engineering tolerance. This revised modal approach is also much simpler to apply and, therefore, should be much less demanding on the computer resources than is the FEM, especially at higher frequencies.

The dimensional analysis is performed to establish an empirical framework for predicting the abovementioned complex ratio. The maximum deviation of the corresponding predictions is ~6% of that estimated using the finite-element simulation. Relatively larger deviations are found when the dominant acoustic mode tends to create a less uniform pressure distribution at the slot. This framework is tested against ducts with a different cross section aspect ratio and a similar level of deviation is observed, suggesting that the present simplified approach is useful for rectangular duct-like structure–cross sections having aspect ratios fall between 0.89 and 2.39.

Whereas it should be noted that the slot opening in the present study is at the corner of a duct-like structure cross section, it is believed that the present simplified approach should be applicable for the slots opened at other parts of the structure wall. The constants in the prediction framework are believed to be slot position dependent.

APPENDIX A: DERIVATION OF EQ. (4)

The sound source in the present study is a vibrating circular piston of radius R flush-mounted on the top of an infinite rectangular duct with height a and width b (Fig. 1). Because the source is mounted on the upper wall,

$$x' = r\cos\theta, \quad y' = \frac{b}{2} + r\sin\theta, \quad \text{and} \quad z' = a. \tag{A1}$$

For the case of rigid duct walls,

$$\begin{aligned}
&\oint \psi_{mn}(y', z') e^{-ik_x(x-x')} dS \\
&= (-1)^m \int_0^R \int_0^{2\pi} \sqrt{(2-\delta_{0m})(2-\delta_{0n})} \\
&\quad \times \cos\left(\frac{n\pi y'}{b}\right) e^{-ik_x(x-x')} r\, d\theta\, dr \\
&= \sqrt{(2-\delta_{0m})(2-\delta_{0n})}(-1)^m e^{-ik_x x} \\
&\quad \times \int_0^R \int_0^{2\pi} \cos\left(k_{0n}\left(\frac{b}{2} + r\sin\theta\right)\right) e^{ik_x r\cos\theta}\, d\theta\, dr.
\end{aligned} \tag{A2}$$

The double integral in Eq. (A2) can be analytically solved by first observing that

$$\begin{aligned}
&\int_0^{2\pi} \cos\left(k_{0n}\left(\frac{b}{2} + r\sin\theta\right)\right) e^{ik_x r\cos\theta} d\theta \\
&= \int_0^{2\pi} \left(\cos\left(\frac{n\pi}{2}\right)\cos(k_{0n} r\sin\theta)\right. \\
&\quad \left. -\sin(k_{0n} r\sin\theta)\sin\left(\frac{n\pi}{2}\right)\right) e^{ik_x r\cos\theta} d\theta \\
&= \begin{cases} 0, & \text{for odd } n, \\ (-1)^{n/2} \int_0^{2\pi} \cos(k_{0n} r\sin\theta) e^{ik_x r\cos\theta} d\theta, & \text{for even } n, \end{cases}
\end{aligned} \tag{A3}$$

as

$$\int_0^{2\pi} \sin(k_{0n} r\ \sin\ \theta)\sin\left(\frac{n\pi}{2}\right) e^{ik_x r\cos\theta}\, d\theta = 0 \tag{A4}$$

for all n. It can be shown using Eq. (A4) and Clause 8.411-1 of Gradshteyn and Ryzhik[24] that

$$\begin{aligned}
&\int_0^{2\pi} \cos(k_{0n} r\ \sin\ \theta) e^{ik_x r\cos\theta}\, d\theta \\
&= \int_{-\pi}^{\pi} e^{i(k_x r\cos\theta + k_{0n} r\sin\theta)} d\theta \\
&= \int_{-\pi}^{\pi} e^{ir\sqrt{k_x^2+k_{0n}^2}\sin\theta}\, d\theta = 2\pi J_0\left(r\sqrt{k_x^2+k_{0n}^2}\right),
\end{aligned} \tag{A5}$$

where J_0 is the Bessel function of zeroth order. By Clause 6.561-5 of Gradshteyn and Ryzhik,[24] one obtains

$$\int_0^R r J_0\left(r\sqrt{k_x^2+k_{0n}^2}\right) dr = \frac{R}{\sqrt{k_x^2+k_{0n}^2}} J_1\left(R\sqrt{k_x^2+k_{0n}^2}\right), \tag{A6}$$

and can then proceed to obtain Eq. (4).

APPENDIX B: CLOSE FORMS OF DOUBLE INTEGRALS IN EQ. (7)

The force, F_j, acting on a piston flush-mounted at an upper corner of the duct cross section at $x = x_j > R$ resulting from the sound source in the present study is given by Eq. (7a),

https://doi.org/10.1121/10.0007061

$$
\begin{aligned}
F_j &= \int_{x_j-w/2}^{x_j+w/2}\int_{a-h}^{a} p(x,0,z)\,dz\,dx \\
&= \int_{-w/2}^{w/2}\int_{a-h}^{a} \frac{\pi\rho\omega RV}{ab}\sum_{m,n}\sqrt{(2-\delta_{0m})(2-\delta_{0n})} \\
&\quad\times \frac{(-1)^{m+n/2}J_1\left(R\sqrt{k^2-k_{m0}^2}\right)}{\sqrt{k^2-k_{mn}^2}\sqrt{k^2-k_{m0}^2}} \\
&\quad\times \psi_{mn}(0,z)e^{-i\omega(x+x_j)/c_{mn}}\,dzdx \\
&= \frac{2\rho\omega RV}{bw}\sum_{m,n} e^{-i\omega x_j/c_{mn}} \\
&\quad\times \frac{(2-\delta_{0m})(2-\delta_{0n})(-1)^{n/2}J_1\left(R\sqrt{k^2-k_{m0}^2}\right)}{\left(k^2-k_{mn}^2\right)\sqrt{k^2-k_{m0}^2}} \\
&\quad\times \frac{\sin\left(\frac{m\pi h}{a}\right)}{m}\sin\left(\frac{w}{2}\sqrt{k^2-k_{mn}^2}\right),
\end{aligned}
\tag{B1}
$$

where n is an even number. The force on the above piston due to its own fluid loading, F_{sj}, is given by Eq. (7b),

$$
\begin{aligned}
F_{sj} &= V_j\int_{x_j-w/2}^{x_j+w/2}\int_{a-h}^{a} M\left(x,0,z|x_j,0,a-h/2\right)dz\,dx \\
&= \frac{\rho\omega hV_j}{ab}\int_{x_j-w/2}^{x_j+w/2}\int_{a-h}^{a}\sum_{m,n}\sqrt{(2-\delta_{0m})(2-\delta_{0n})} \\
&\quad\times \frac{\sin\left(\frac{m\pi h}{a}\right)\left[1-e^{-i\omega w/2c_{mn}}\cos\left(\frac{\omega x}{c_{mn}}\right)\right]}{i(-1)^m\left(\frac{m\pi h}{a}\right)\left(k^2-k_{mn}^2\right)} \\
&\quad\times \psi_{mn}(0,z)\,dz\,dx \\
&= \frac{\rho\omega h^2V_j}{ab}\sum_{m,n}\frac{(2-\delta_{0m})(2-\delta_{0n})\sin^2\left(\frac{m\pi h}{a}\right)}{i\left(\frac{m\pi h}{a}\right)^2\left(k^2-k_{mn}^2\right)} \\
&\quad\times \left[w-\frac{2e^{-i(w/2)\sqrt{k^2-k_{mn}^2}}}{\sqrt{k^2-k_{mn}^2}}\sin\left(\frac{w}{2}\sqrt{k^2-k_{mn}^2}\right)\right].
\end{aligned}
\tag{B2}
$$

Finally, the force on this piston due to the vibration of an identical piston at $x=x_i$, where $|x_i-x_j|>w$, is

$$
\begin{aligned}
F_{mj} &= \sum_{i\neq j}V_i\int_{x_j-w/2}^{x_j+w/2}\int_{a-h}^{a} G(x,0,z|x_i,0,a-h/2)\,dz\,dx \\
&= \frac{\rho\omega h}{ab}\sum_{i\neq j}V_i\int_{x_j-w/2}^{x_j+w/2}\int_{a-h}^{a}\sum_{m,n}\sqrt{(2-\delta_{0m})(2-\delta_{0n})}\frac{\sin\left(\frac{m\pi}{a}h\right)\sin\left(\frac{\omega w}{2c_{mn}}\right)}{(-1)^m\frac{m\pi h}{a}\left(k^2-k_{mn}^2\right)}\psi_{mn}(0,z)e^{-i\omega|x-x_i|/c_{mn}}\,dz\,dx \\
&= \frac{2\rho\omega h^2}{ab}\sum_{i\neq j}\left[V_i\sum_{m,n}\frac{(2-\delta_{0m})(2-\delta_{0n})\sin^2\left(\frac{m\pi h}{a}\right)\sin^2\left(\frac{w}{2}\sqrt{k^2-k_{mn}^2}\right)}{\left(\frac{m\pi h}{a}\right)^2\left(k^2-k_{mn}^2\right)^{3/2}}e^{-i|x_j-x_i|\sqrt{k^2-k_{mn}^2}}\right].
\end{aligned}
\tag{B3}
$$

[1]A. Fry, *Noise Control in Building Services* (Pergamon, Oxford, 1988), Chap. 7.
[2]H. G. Davies, "Noise propagation in corridors," J. Acoust. Soc. Am. **53**, 1253–1262 (1973).
[3]See https://zenithfilms.com.sg/hdb-corridor-window-privacy-singapore-homes/, http://blog-imgs-44.fc2.com/m/a/r/maritaso303monozuki/6mR9HM2mPR19Wlt_1349234745.jpg and https://pbs.twimg.com/media/CLnsMCPVAAAcIgD.jpg (Last viewed December 31, 2020).
[4]R. K. Kwan, "Train noise in 3-D consideration," in *Proc*eedings of *InterNoise 2009*, Ottawa, Canada (2009), Paper no. 795.
[5]R. Xiao, P. Joseph, and J. Li, "The leak noise spectrum in gas pipeline systems: Theoretical and experimental investigation," J. Sound Vib. **488**, 115646 (2020).
[6]Q. Xu, L. Zhang, and W. Liang, "Acoustic detection technology for gas pipeline leakage," Process Saf. Environ. Prot. **91**, 253–261 (2013).
[7]P. J. Lee, J. P. Vítkovský, M. F. Lambert, A. R. Simpson, and J. A. Liggett, "Leak location using the pattern of the frequency response diagram in pipelines: A numerical study," J. Sound Vib. **284**, 1051–1073 (2005).
[8]J. Lin, X. Wang, and M. S. Ghidaoui, "Theoretical investigation of Leak's impact on normal modes of a water-filled pipe: Small to large leak impedance," J. Hydraul. Eng. **145**, 04019017 (2019).
[9]C. Capponi, S. Meniconi, and B. Brunone, "Discussions of 'theoretical investigation of Leak's impact on normal modes of a water-filled pipe: Small to large leak impedance' by Jingrong Lin, Xun Wang and Mohamed S. Ghidaoui," J. Hydraul. Eng. **147**, 07020013 (2021).
[10]A. Cummings, "The attenuation of lined plenum chambers in ducts: I. Theoretical analysis," J. Sound Vib. **61**, 347–- 373 (1978).
[11]Y. J. Tang and S. K. Tang, "On low frequency sound propagation across closely coupled narrow cavities along an infinite duct and the similarity in stopband cut-on frequencies," J. Sound Vib. **443**, 411–429 (2019).
[12]C. R. Hart and S. K. Lau, "Active noise control with linear control source and sensor arrays for a noise barrier," J. Sound Vib. **331**, 15–26 (2012).
[13]S. K. Tang, "Narrow sidebranch arrays for low frequency duct noise control," J. Acoust. Soc. Am. **132**, 3086–3097 (2012).
[14]S. K. Tang, "On sound transmission loss across a Helmholtz resonator in a low Mach number flow duct," J. Acoust. Soc. Am. **127**, 3519–3525 (2010).

[15]COMSOL, *COMSOL Multiphyiscs User Guide* (COMSOL AB, Stockholm, Sweden, 2012).
[16]Q. H. Liu, "Perfectly matched layers for elastic waves in cylindrical and spherical coordinates," J. Acoust. Soc. Am. **105**, 2075–2084 (1999).
[17]S. Marburg, "Six boundary elements per wavelength: Is that enough?," J. Comput. Acoust. **10**, 25–51 (2002).
[18]L. E. Kinsler, A. R. Frey, A. B. Coppens, and J. V. Sanders, *Fundamentals of Acoustics*, 4th ed. (Wiley, New York, 2000), Chap. 10.
[19]P. M. Morse and K. U. Ingard, *Theoretical Acoustics* (McGraw Hill, New York, 1968), pp. 393–394.
[20]P. Joseph, C. L. Morfey, and C. R. Lowis, "Multi-mode sound transmission in ducts with flow," J. Sound Vib. **264**, 523–544 (2003).
[21]H. H. Huang, X. J. Qiu, and J. Kang, "Active noise attenuation in plenum windows," J. Acoust. Soc. Am. **130**, 176–188 (2011).
[22]P. E. Doak, "Excitation, transmission and radiation of sound from source distributions in hard-walled ducts of finite length (I): The effects of duct cross-section geometry and source distribution space-time pattern," J. Sound Vib. **31**, 1–72 (1973).
[23]M. C. Junger and D. Feit, *Sound, Structures, and Their Interaction* (MIT Press, Cambridge, 1986), Chap. 8.
[24]I. S. Gradshteyn and I. M. Ryzhik, *Tables of Integrals, Series and Products* (Academic, London, 1980).